



Published in final edited form as:

*IEEE Trans Biomed Eng.* 2013 June ; 60(6): 1735–1741. doi:10.1109/TBME.2013.2241764.

## An Approach to Rapid Calculation of Temperature Change in Tissue Using Spatial Filters to Approximate Effects of Thermal Conduction

**Giuseppe Carluccio [Member, IEEE],**

Department of Radiology, New York University, New York, NY 10016 USA

**Danilo Erricolo [Senior Member, IEEE],**

Department of Electrical and Computer Engineering, University of Illinois at Chicago, Chicago, IL 60607 USA

**Sukhoon Oh, and**

Department of Radiology, New York University, New York, NY 10016 USA

**Christopher M. Collins [Senior Member, IEEE]**

Department of Radiology, New York University, New York, NY 10016 USA

Giuseppe Carluccio: giuseppe.carluccio@nyumc.org; Danilo Erricolo: erricolo@ece.uic.edu; Sukhoon Oh: sukhoon.oh@nyumc.org; Christopher M. Collins: c.collins@nyumc.org

### Abstract

We present an approach to performing rapid calculations of temperature within tissue by interleaving, at regular time intervals, 1) an analytical solution to the Pennes (or other desired) bioheat equation excluding the term for thermal conduction and 2) application of a spatial filter to approximate the effects of thermal conduction. Here, the basic approach is presented with attention to filter design. The method is applied to a few different cases relevant to magnetic resonance imaging, and results are compared to those from a full finite-difference (FD) implementation of the Pennes bio-heat equation. It is seen that results of the proposed method are in reasonable agreement with those of the FD approach, with about 15% difference in the calculated maximum temperature increase, but are calculated in a fraction of the time, requiring less than 2% of the calculation time for the FD approach in the cases evaluated.

### Index Terms

Calculation; filter; magnetic resonance imaging (MRI); specific energy absorption rate (SAR); temperature

## I. Introduction

In a number of biomedical applications, a change in the energy deposition throughout the body can lead to a change in the temperature distribution. In many cases, it is advantageous to predict the temperature change from estimates of the energy distribution in order to assure, depending on the particular application, that a desired temperature distribution is achieved [1]–[3] or that no tissues will be heated excessively [4]–[6].

Currently in magnetic resonance imaging (MRI), there is great interest in performing case-specific safety evaluations very rapidly. This is in part due to the development of transmit arrays in MRI [7], facilitating an infinite variety of possible desired radiofrequency (RF) magnetic field patterns and associated RF heating patterns in each individual patient. One major challenge to real-time case-specific safety predictions is accurate prediction of the heating pattern, or specific energy absorption rate (SAR) distribution in the subject. While there are a variety of approaches to calculating [8], [9] or measuring [10], [11] this pattern with increasing speed, another obstacle is the interpretation of the SAR distribution for purposes of ensuring safety. Although exposure to increased temperature over time is more easily correlated with potential damage to tissue [12], due in part to complexities and time requirements for calculating temperature, a spatially averaged SAR value, often averaged over 10 g regions ( $\text{SAR}_{10g}$ ), is used much more commonly in safety evaluations.

Recently, methods to rapidly compute temperature increase for biomedical applications have been included [13]–[15]: a hybrid alternating-direction implicit (ADI) approach to solving the heat equation for a heterogeneous numerical model [13], a method of superposition from separate sources combined with model simplification [14], and a semianalytical Fourier-based solution for simple 3-D geometry [15]. Here, we present a new accelerated approach to solving the Pennes (or other) bioheat equation. Recognizing that thermal conduction—the most computationally intensive portion of models for heat transfer in biological samples—has the effect of smoothing or blurring the temperature distribution in space, we approximate the effects of thermal conduction with a low-pass spatial filter applied to the temperature distribution at regular time intervals. The method produces reasonably accurate results much more quickly than the more commonly used finite-difference (FD) approach to calculating temperature, and even more quickly than calculation of complete  $\text{SAR}_{10g}$  distribution. It is hoped that this approach will be useful in rapid production of meaningful evaluations of heat induced during MRI and other applications in the future.

## II. Method

### A. Temperature Computation

The relationship between temperature  $T$  and the applied energy distribution is often described with Pennes' bioheat equation [16]

$$\rho c_h \frac{\partial T}{\partial t} = \nabla \cdot (k \nabla T) - W_{\rho_{bl} c_{hbl}} (T - T_{bl}) + Q + \rho \text{SAR} \quad (1)$$

where  $c_h$  is the heat capacity,  $W$  is the blood perfusion rate,  $k$  is the thermal conductivity,  $\rho$  is the tissue mass density, the subscript  $bl$  indicates values for blood,  $Q$  is the heat generated by metabolism, and SAR is the specific energy absorption rate (W per kg of tissue) resulting from some heating source. For example, in the case of RF electromagnetic field with rms electric field  $E$

$$\text{SAR} = \frac{\sigma |E|^2}{\rho} \quad (2)$$

where  $\sigma$  is the electrical conductivity.

While Pennes' bioheat equation has its limitations, it is often used as a good first-order approximation for temperature in tissue. The largest computational challenge to applying (1) is the time required to accurately calculate the thermal conduction of heat, represented by the first term on the right-hand side of the equation.

Separating  $T$  in (1) into an initial equilibrium temperature  $T_0$  when SAR is zero and a time-dependent increased temperature  $T_i$  after perturbation with a nonzero SAR such that  $T = T_0 + T_i$ , we can write

$$\rho c_h \frac{\partial T_0}{\partial t} + \rho c_h \frac{\partial T_i}{\partial t} = \nabla \cdot (k \nabla T_0) + \nabla \cdot (k \nabla T_i) - W \rho_{bl} c_{hbl} (T_0 - T_{bl}) - W \rho_{bl} c_{hbl} T_i + Q + \rho \text{SAR} \quad (3)$$

and

$$\rho c_h \frac{\partial T_0}{\partial t} = \nabla \cdot (k \nabla T_0) - W \rho_{bl} c_{hbl} (T_0 - T_{bl0}) + Q_0. \quad (4)$$

Subtracting (4) from (3) produces

$$\rho c_h \frac{\partial T_i}{\partial t} = \nabla \cdot (k \nabla T_i) - W \rho_{bl} c_{hbl} (T_i) + \rho \text{SAR} + \Delta Q + W \rho_{bl} c_{hbl} \Delta T_{bl} \quad (5)$$

where  $Q = Q_0 + \Delta Q$  and  $T_{bl} = T_{bl0} + \Delta T_{bl}$  and where, for the linearity of (5),  $\Delta Q$  and  $\Delta T_{bl}$  can be considered as an additional heat sources (or sinks, depending on the sign of these terms) like SAR.

If absolute temperature (rather than just temperature change) is desired,  $T_0$  needs to be calculated only once for a given biological sample with any desired method, such as a full FD implementation of (1) [4]. Conceivably, experimentally measured data could also be used to provide the initial equilibrium temperature distribution. Depending on the application, it may be necessary to calculate only the temperature increase above  $T_0$  (i.e.,  $T_i$ ) in which case only (5) is needed. Using a similar approach, we can also consider the increase in temperature in multiple stages or intervals  $n$  such that  $T_{n+1} = T_n + \Delta T_n$  where  $\Delta T_n$  is the temperature increase during the  $n^{\text{th}}$  time interval.

With our proposed approach,  $T_i$  over time is calculated by applying a spatial filter at regular intervals  $t_{\text{int}}$  to approximate effects of thermal conduction (the first term on the right-hand side of (5)) and calculating the effects of the remaining terms in (5) over the same intervals analytically. If the thermal conduction term is removed from (5), what remains is a first-order linear ordinary differential equation

$$T_{n+1} = \frac{\rho \text{SAR} + \Delta Q + W \rho_{\text{bl}} c_{\text{hbl}} \Delta T_{\text{bl}}}{W c_{\text{bl}} \rho_{\text{bl}}} \left( 1 - e^{-\frac{W c_{\text{hbl}} \rho_{\text{bl}}}{c_{\text{h}} \rho} t_{\text{int}}} \right) + T_n e^{-\frac{W c_{\text{hbl}} \rho_{\text{bl}}}{c_{\text{h}} \rho} t_{\text{int}}} \quad (6)$$

and can be solved directly. Importantly, all parameters in this equation (especially  $Q$ ,  $T_{\text{bl}}$ , and  $W$ ) can be considered functions of time or local temperature and updated according to additional considerations, such as thermoregulation [6].

To design an effective spatial filter for accurately approximating the effects of thermal conduction, we selected an approach considering the poles of a 3-D low-pass filter

$$F(\lambda_x, \lambda_y, \lambda_z) = \frac{1}{\left(1 + \frac{i\lambda_x}{p_{x1}}\right)^{\alpha_{x1}} \left(1 + \frac{i\lambda_x}{p_{x2}}\right)^{\alpha_{x2}} \left(1 + \frac{i\lambda_y}{p_{y1}}\right)^{\alpha_{y1}}} \cdot \frac{1}{\left(1 + \frac{i\lambda_y}{p_{y2}}\right)^{\alpha_{y2}} \left(1 + \frac{i\lambda_z}{p_{z1}}\right)^{\alpha_{z1}} \left(1 + \frac{i\lambda_z}{p_{z2}}\right)^{\alpha_{z2}}} \quad (7)$$

where  $\lambda_x$ ,  $\lambda_y$ , and  $\lambda_z$  are the spatial variables in the Fourier domain corresponding to  $x$ ,  $y$ , and  $z$  directions, respectively;  $p_{x1}$ ,  $p_{y1}$ , and  $p_{z1}$  are the first (low) cutoff frequencies for the spatial variables  $\lambda_x$ ,  $\lambda_y$ ,  $\lambda_z$ ; and  $p_{x2}$ ,  $p_{y2}$ , and  $p_{z2}$  the second (high) cutoff frequencies in the Fourier directions. Two cutoff frequencies in each direction have been chosen, due to the spatial second derivative dependence of heat conductivity in (5). In addition,  $\alpha_{x1}$ ,  $\alpha_{y1}$ , and  $\alpha_{z1}$  are the orders of the first cutoff frequencies, and  $\alpha_{x2}$ ,  $\alpha_{y2}$ , and  $\alpha_{z2}$  the orders of the second cutoff frequencies. The parameters  $\alpha$  and  $p$  change according to the user-selected time interval  $t_{\text{int}}$ .

Using the properties of the Fast Fourier Transform (FFT), the cutoff frequencies in (7) can be scaled appropriately for the size of the meshgrid (dimensions of the sample space in grid cells) and meshgrid dimensions (size of a single cell in meters). In fact, the cutoff frequency is proportional to the size of the meshgrid and to the meshgrid dimensions. For example, if we indicate with  $M_{m \times n \times p}$  the size of the meshgrid containing the sample, and with  $a$ ,  $b$ , and  $c$  the dimensions of the grid in the  $x$ ,  $y$ , and  $z$  directions

$$\begin{aligned} p_{x1} &= p_{x1s} \frac{ma}{m_s a_s} \\ p_{x2} &= p_{x2s} \frac{ma}{m_s a_s} \\ p_{y1} &= p_{y1s} \frac{nb}{n_s b_s} \\ p_{y2} &= p_{y2s} \frac{nb}{n_s b_s} \\ p_{z1} &= p_{z1s} \frac{pc}{p_s c_s} \\ p_{z2} &= p_{z2s} \frac{pc}{p_s c_s} \end{aligned} \quad (8)$$

where  $p_{x1s}$ ,  $p_{x2s}$ ,  $p_{y1s}$ ,  $p_{y2s}$ ,  $p_{z1s}$ , and  $p_{z2s}$  are the computed optimum cutoff frequencies for starting matrix  $M_s$  of dimensions  $m_s \times n_s \times p_s$  ( $M_{s, m_s, n_s, p_s}$ ) with meshgrid resolution  $a_s \times b_s \times c_s$ .

In this study, the optimal values for all cutoff frequencies  $p$  and orders  $\alpha$  were determined for three different time intervals  $t_{\text{int}}$  (30, 60, and 120, s) using a conjugate gradient method to minimize the sum of the square of the difference in temperature between the result applying the filter and that calculated using an FD solution of (1) [8] for a box-shaped sample of water at  $2 \text{ mm} \times 2 \text{ mm} \times 2 \text{ mm}$  resolution and an SAR distribution determined numerically using commercial software (XFDTD, Remcom Inc., State College, PA) for the sample in a birdcage coil for MRI at 125 MHz. Details of the model and validation of the full FD heating pattern with comparison to experiment have been published previously [17]. In the determination of SAR, the sample was assigned an electrical conductivity of 1.895 S/m, and a relative electric permittivity of 78.

After the optimal parameters were determined, the ability to scale them according to mesh spatial resolution as in (8) was tested with a variety of applications in comparison to a full FD representation of (1). These included a human head in a quadrature surface coil for MRI at 300 MHz [8] and a human head with a 5 mm focal heating source in brain, as might more be pertinent in a model for ablation.

Starting from the temperature distribution  $T_n = T_0$ , the procedure to apply the method can be summarized as the application of following.

*Step 1:* the solution given in (6) of the analytical equation (5) without the heat conductivity term.

*Step 2:* computation of the FFT of the temperature distribution  $T_{n+1}$ .

*Step 3:* application of the filter in (7).

*Step 4:* computation of the inverse FFT.

The procedure is repeated until the total heating time is computed, defining  $T_n$  as the solution of the inverse FFT (Step 4) at the end of each repetition.

## B. SAR<sub>10g</sub> Computation

To compare temperature distributions to the corresponding SAR<sub>10g</sub> distributions, we utilized a previously presented method for calculating SAR<sub>10g</sub> [20], [21]. The algorithm sequentially increases the radius of a spherical mask centered on the voxel of interest. The mass and the summed SAR of all the voxels in both the most external layer and the interior volume are calculated. When the total mass (external layer plus inner ones) exceeds 10 g, the SAR of the external layer is weighted to reach the desired 10 g mass. Indicating with  $m_s$  and  $m_i$  the mass in grams of the surface and interior portions, respectively, SAR<sub>s</sub> and SAR<sub>i</sub> the sum of the SAR values in the external and internal layers respectively, and  $n_s$  and  $n_i$  the number of pixels in the external and internal layers, the SAR<sub>10g</sub> is calculated as

$$\text{SAR}_{10g} = \frac{\left(\frac{10g - m_i}{m_s}\right) \text{SAR}_s + \text{SAR}_i}{\left(\frac{10g - m_i}{m_s}\right) n_s + n_i}. \quad (9)$$

### III. Results

Table I provides the empirically determined optimal values for the filter parameters on a matrix of 250 cells in each dimension ( $M_{s250, 250, 250}$ ) with a resolution of 2 mm in each dimension ( $a_s = b_s = c_s = 2$  mm) and for a variety of time intervals. As discussed previously, cutoff frequencies  $p$  for (7) can easily be determined for other sample sizes and grid resolutions (8) and the orders  $a$  for (7) are independent of these parameters, but the optimal values must be determined for each time interval independently.

Fig. 1 presents the results for the case of a gelatinous phantom exposed to an SAR distribution as induced by a birdcage-type MRI coil [17] designed for imaging of the human head. Figs. 2 and 3 similarly present the geometry and results for the case of a human head exposed to an SAR distribution induced by a quadrature surface coil for MRI [8], and a point source of heat deep within brain tissue (more relevant for local ablation than MRI), respectively. The material properties used for the cases of the head model are reported in Table II. In each of these three figures, the unaveraged SAR,  $SAR_{10g}$ , temperature increases as calculated with the full FD and proposed methods, and the differences between these last two are presented. For each case shown here, the time required to calculate temperature with the proposed method was tens of seconds depending on the meshgrid resolution, matrix size, and total heating time for a 3 GHz central processing unit (CPU) with 4 GB of random access memory (RAM). The computation time is less than 2% of that required to calculate temperature with the full FD method and less than 10% of that required to calculate  $SAR_{10g}$  (see Figs. 1–3).

### IV. Discussion

The distribution of temperature increase resulting from the application of heat *in vivo* is a function of many factors that can be considered dependent on temperature and/or environment, including rates of blood perfusion and metabolism throughout the body and rates of perspiration and radiation at the surface of the body [5], [6]. Additionally, the directionality of blood flow through a heat field adds significant complexity, especially near blood vessels [18], [19].

Any accurate prediction of temperature *in vivo* must consider effects of thermal conduction. In the Pennes bioheat equation (a well-known, relatively simple formula for calculating temperature), the term for heat conduction is the most complex and difficult to calculate. Here, we have shown that approximating the effects of this term with a spatial filter can greatly accelerate the calculation of temperature increase while still producing reasonable results when compared to a full FD approach. Success of this approach stems, in part, from the fact that thermal conductivity in human tissues, in comparison to perfusion rates and rates of metabolism, are relatively homogeneous [8]. While the application of the spatial filter approximation used here was to the Pennes bioheat equation, in principle it could be integrated into more sophisticated representations to accelerate the estimation of thermal conduction effects.

In the applications presented here, two are related to assessing the amount of RF heating occurring during an MRI exam (see Figs. 1 and 2) and one is more closely related to

localized ablation (see Fig. 3). In the case of a nonperfused imaging phantom within an MRI coil (see Fig. 1), the proposed method gives results within about 0.15 °C of the full FD calculation, or within about 8% of the maximum temperature increase. In the case of a perfused human head within an MRI coil (see Fig. 2), the proposed method gives results within about 0.075 °C of the full FD calculation, or within about 15% of the maximum temperature increase. In both of these cases, the proposed method overestimates the maximum temperature increase, which would provide a more conservative estimate for safety assurance. In the case of a perfused human head with a local heat source deep in the brain (see Fig. 3), the proposed method gives results within about 0.05 °C of the full FD calculation, or within about 3% of the maximum temperature increase. In this case, the proposed method underestimates and overestimates temperature increase by nearly equal amounts and in nearly equal volumes throughout space. The amount of relative error in the case of the local source deep in brain is lowest because here the greatest amount of heating occurs at a location surrounded by tissue with fairly homogeneous thermal conductivity. The case of the human head in the MRI coil has the largest relative error because the location of greatest temperature increase occurs near a boundary between tissues of dissimilar thermal conductivities. Therefore, the use of the method is not suggested in applications where the volumes of interest is very small and in contact with the air, such as small extremities of small animals. On the contrary, the speed of the method and its accuracy when used with human body tissues may suggest its use as part of a real-time MRI scan protocol.

While there are some minor differences between the results produced with the fast spatial filter approximation and those from the full FD approach, it is clear that the results provide information much more directly relevant to safety and tissue damage than does  $SAR_{10g}$  [12]. Because the proposed method also requires less time than is required to calculate the  $SAR_{10g}$  throughout the sample, it is hoped that the obstacles to calculating temperature distribution for evaluation of safety will seem significantly reduced so that temperature will be calculated more often.

## V. Conclusion

We have presented a new method for fast calculation of temperature in tissue samples by replacing the term for thermal conduction with a spatial filter. The approach produces results in good general agreement with full FD calculations of temperature, but requires much less computation time.

## Acknowledgments

This work was supported in part by the U.S. National Institutes of Health under Grant EB000454.

## References

1. Labonte S. A computer simulation of radio-frequency ablation of the endocardium. *IEEE Trans Biomed Eng.* Sep; 1994 41(9):883–890. [PubMed: 7959815]
2. Sullivan D. Three-dimensional computer simulation in deep regional hyperthermia using the finite-difference time-domain method. *IEEE Trans Microw Theory Tech.* Feb; 1990 38(2):204–211.

3. Wust P, Seebass M, Nadobny J, Deuffhard P, Monich G, Felix R. Simulation studies promote technological development of radiofrequency phased array hyperthermia. *Int J Hypertherm.* 1996; 12:477–494.
4. Collins CM, Liu W, Wang JH, Gruetter R, Vaughan JT, Ugurbil K, Smith MB. Temperature and SAR calculations for a human head within volume and surface coils at 64 and 300 MHz. *J Magn Reson Imag.* 2004; 19:650–656.
5. Bernardi P, Cavagnero M, Pisa S, Piuze E. Specific absorption rate and temperature elevation in a subject exposed in the far-field of radio-frequency sources operating in the 10–900 MHz range. *IEEE Trans Biomed Eng.* Mar; 2003 50(3):295–303. [PubMed: 12669986]
6. Wang Z, Lin JC, Vaughan JT, Collins CM. Consideration of physiological response in numerical models of temperature during MRI of the human head. *J Magn Reson Imag.* 2008; 28:1303–1308.
7. Zhu Y. Parallel excitation with an array of transmit coils. *Magn Reson Med.* Apr.2004 51:775–784. [PubMed: 15065251]
8. Collins CM, Li S, Smith MB. SAR and  $B_1$  field distributions in a heterogeneous human head model within a birdcage coil. *Magn Reson Med.* 1998; 40:847–856. [PubMed: 9840829]
9. van den Berg CAT, van den Bergen B, van de Kamer JB, Raaymakers BW, Kroeze H, Bartels LW, Lagendijk JJW. Simultaneous B homogenization and specific absorption rate hotspot suppression using a magnetic resonance phased array transmit coil. *Magn Reson Med.* 2007; 57:577–586. [PubMed: 17326185]
10. Shapiro EM, Borthakur A, Reddy R. MR imaging of RF heating using a paramagnetic doped agarose phantom. *MAGMA.* 2000; 10:114–121. [PubMed: 10873201]
11. Cao, Z.; Oh, S.; Ehses, P.; Carluccio, G.; Collins, CM.; Griswold, MA. An in vivo study on fast PRF temperature imaging based on compressed sensing: An alternative approach to monitor RF safety?. *Proc. ISMRM 21st Annu. Meeting; Melbourne, Australia.* 2012; p. 312
12. Yarmolenko PS, Moon EJ, Landon C, Manzoor A, Hochman DW, Viglianti BL, Dewhirst MW. Thresholds for thermal damage to normal tissues: An update. *Int J Hypertherm.* Jun.2011 27:320–343.
13. Singh V, Roy A, Castro R, McClure K, Dai R, Agrawal R, Greenberg RJ, Weiland JD, Humayun MS, Lazzi G. On the thermal elevation of a 60-electrode Epi-retinal prosthesis to restore partial vision to the blind. *IEEE Trans Biomed Circuits Syst.* Dec; 2008 2(4):289–300. [PubMed: 23853132]
14. Das SK, Clegg ST, Samulski TV. Computational techniques for fast hyperthermia temperature optimization. *Med Phys.* Feb; 1999 26(2):319–328. [PubMed: 10076991]
15. Dillenseger J, Esneault S. Fast FFT-based bioheat transfer equation computation. *Comput Biol Med.* 2010; 40(2):119–123. [PubMed: 20018277]
16. Pennes HH. Analysis of tissue and arterial blood temperatures in the resting human forearm. *J Appl Physiol.* 1948; 1:93–122. [PubMed: 18887578]
17. Oh S, Webb AG, Neuberger T, Park B, Collins CM. Experimental and numerical assessment of MRI-induced temperature change and SAR distributions in phantoms and in vivo. *Magn Reson Med.* 2010; 63:218–223. [PubMed: 19785018]
18. Van Leeuwen GM, Hand JW, Lagendijk JJW, Azzopardi DV, Edwards AD. Numerical modeling of temperature distributions within the neonatal head. *Pediatr Res.* 2000; 48:351–356. [PubMed: 10960502]
19. Craciunescu OI, Raaymakers BW, Kotte AN, Das SK, Samulski TV, Lagendijk JJW. Discretizing large traceable vessels and using DEMRI perfusion maps yields numerical temperature contours that match the MR noninvasive measurements. *Med Phys.* 2001; 28:2289–2296. [PubMed: 11764035]
20. Oh, S.; Carluccio, G.; Collins, CM. Method and tool for improved, rapid n-gram average SAR determination,” in. *Proc. 19th Annu. Meeting ISMRM; Montreal, Canada.* 2011; p. 3868
21. Carluccio, G. Doctoral dissertation. Univ. Illinois at Chicago; Chicago, IL, USA: 2011. Locally optimized  $B_1$  field for MRI systems.



## Biographies



**Giuseppe Carluccio** (M'11) received the Laurea degree (*summa*) and the Laurea Specialistica degree (*summa cum laude*) both in electronics engineering from the Politecnico di Milano, Milan, Italy, in 2005 and 2010, respectively, and the M.Sc. and Ph.D. degrees in electrical and computer engineering from the University of Illinois at Chicago (UIC), Chicago, USA, in 2011.

His research interests include applied electromagnetic, specifically waves propagation in biological tissues, RF shimming in magnetic resonance imaging, safety in magnetic resonance imaging, and temperature increase in biological tissues. He is currently a Postdoctoral Fellow in the Department of Radiology, New York University, New York, USA.

Dr. Carluccio received the 2011 Provost and Deiss Award at the UIC.



**Danilo Erricolo** (S'97–M'99–SM'03) received the Laurea degree (*summa cum laude*) in electronics engineering from the Politecnico di Milano, Milano, Italy, in 1993, and the Ph.D. degree in electrical engineering and computer science from the University of Illinois at Chicago (UIC), Chicago, USA, in 1998.

He is currently a Professor with the Department of Electrical and Computer Engineering, UIC, where he is also the Director of the Andrew Electromagnetics Laboratory. He has authored or coauthored more than 170 publications in refereed journals and international conferences. In 2009, he was a U.S. Air Force Summer Faculty Fellow. His primary research interests include electromagnetic scattering, magnetic resonance imaging, radar, wireless communications, and electromagnetic compatibility. His research activity has been supported by the Department of Defense and the National Science Foundation.

Dr. Erricolo is a member of Eta Kappa Nu and was elected a full member of Commissions B, C, and E of the U.S. National Committee of the International Union of Radio Science (USNC-URSI), a committee of the National Academies. He served for USNC-URSI

Commission E as Secretary (2004–2005), Vice-Chair (2006–2008), and Chair (2009–2011); since 2009, he has been serving as the Chair of the USNC-URSI Ernest K. Smith Student Paper Competition, and he was an elected Member at Large of USNC-URSI for the triennium 2012–2014. He is an Associate Editor for the IEEE ANTENNAS AND WIRELESS PROPAGATION LETTERS. He was the Vice-Chair of the Local Organizing Committee of the XXIX URSI General Assembly (Chicago, IL, USA, August 7–16, 2008) and the General Chair of the 2012 IEEE Antennas and Propagation International Symposium/USNC National Radio Science Meeting (Chicago, IL, USA, July 8–14, 2012). He was elected as a member of the Administrative Committee of the IEEE Antennas and Propagation Society for the triennium 2012–2014.



**Sukhoon Oh** received the B.S. degree from KonKuk University, Seoul, Korea, in 1998, and the Ph.D. degree from Kyung Hee University, Seoul, in 2006, both in biomedical engineering. During his doctoral study, his research was focused mainly on magnetic resonance electric impedance tomography, working to show a cross-sectional image of electric conductivity and permittivity for tumor detection in the human body.

He has been a Research Associate at the Center for NMR Research (CNMRR), Pennsylvania State University, University Park, USA, since 2008 after his postdoctoral training (2006–2008) at the CNMRR, where he extended his research area to the electromagnetic (EM) field simulations of RF coils, including transmit array coils. Recently, he has been involved in developing and/or performing temperature and specific energy absorption rate (SAR) mapping of various MR safety related issues by using both MR imaging EM field simulations. He is currently a Research Assistant at the Center for Biomedical Imaging, New York University Langone Medical Center (NYU), New York, USA. At NYU, he continues his research about the effect of high-dielectric materials on the image signal-to-noise ratio and SAR in a high field-strength (7T) MRI system.



**Christopher M. Collins** (M'00–SM'12) received the Baccalaureate degree in engineering science from The Pennsylvania State University (PSU), University Park, USA, in 1993, and

the Ph.D. degree in bioengineering from The University of Pennsylvania, Philadelphia, USA, in 1999.

He joined the faculty in Radiology at PSU in 2001 after a postdoctoral fellowship there, becoming a Full Professor in 2010. He is currently a Professor of Radiology at the New York University Langone Medical Center, New York, USA, as a member of the Bernard and Irene Schwatz Center for Biomedical Imaging. His research interests include use of numerical methods considering field/tissue interactions to simulate, evaluate, and ensure safety and efficacy of MRI.

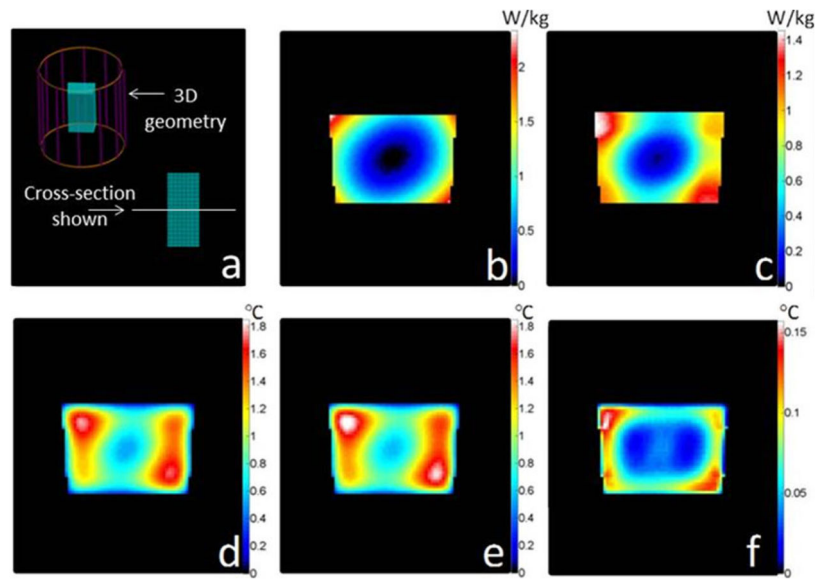


**Fig. 1.**

For a box of water-based gel, plots of (a) geometry of the problem with the box in a birdcage coil operating at 125 MHz, (b) the unaveraged SAR distribution, (c) 10 g average SAR distribution (1 min computation time), (d) temperature increase calculated with a rigorous FD algorithm (15 min heating time, 6 min computation time), (e) temperature increase calculated with the proposed rapid algorithm (15 min heating time, 5 s computation time), and (f) difference between the full FD method and the proposed method. The chosen time interval is  $t_{\text{int}} = 30$  s, the meshgrid resolution is  $2 \text{ mm} \times 2 \text{ mm} \times 2 \text{ mm}$ , and the matrix size is  $80 \times 80 \times 80$  cells.

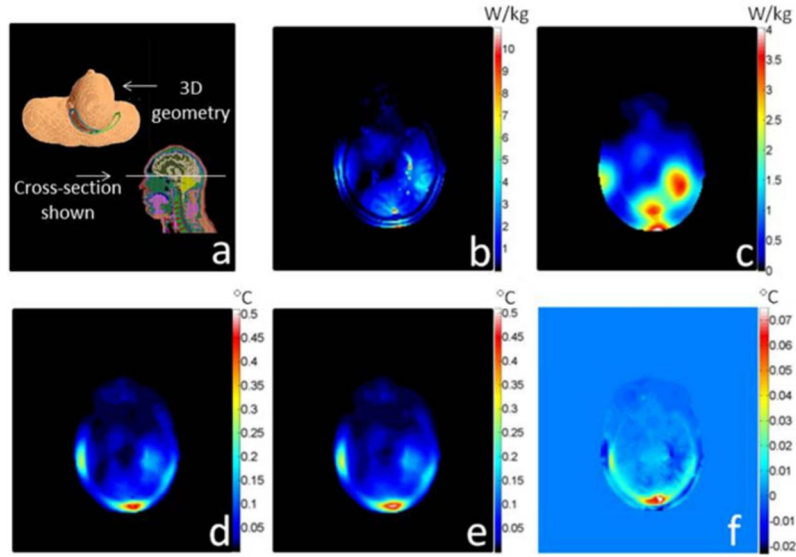


**Fig. 2.** For a human head model, plots of (a) geometry of the problem with the head in a quadrature surface coil operating at 125 MHz, (b) unaveraged SAR distribution, (c) 10 g average SAR distribution (4 min computation time), (d) temperature increase calculated with a rigorous FD algorithm (15 min heating time, 23 min computation time), (e) temperature increase calculated with the proposed rapid algorithm (15 min heating time, 25 s computation time), and (f) the difference between the full FD method and the proposed method. The chosen time interval is  $t_{\text{int}} = 30$  s, the meshgrid resolution is  $2 \text{ mm} \times 2 \text{ mm} \times 2 \text{ mm}$ , and the matrix size is  $150 \times 140 \times 120$  cells.

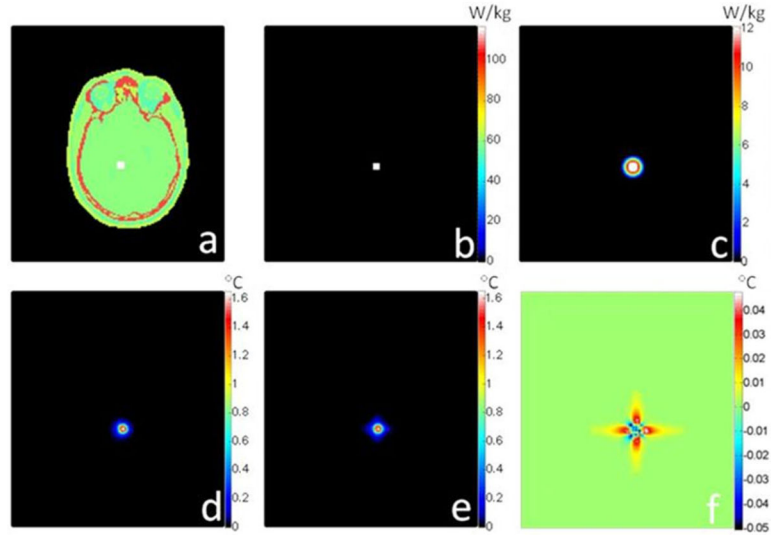


**Fig. 3.** For a human head model, plots of (a) geometry of the problem showing the heat source (white box) within the head (the 3-D geometry and the cross section are the same as Fig. 2), (b) unaveraged SAR distribution, (c) 10 g average SAR distribution(4 min computation time), (d) temperature increase calculated with a rigorous FD algorithm (15 min heating time, 23 min computation time), (e) temperature increase calculated with the proposed rapid digital filter algorithm (15 min heating time, 25 s computation time), and (f) difference maps between the full FD method and the proposed method. The chosen time interval is  $t_{int} = 30$  s, the meshgrid resolution is  $2 \text{ mm} \times 2 \text{ mm} \times 2 \text{ mm}$ , and the matrix size is  $150 \times 140 \times 120$  cells.

TABLE I

## Optimum Filter Parameters

Parameters	$t_{int} = 30s$	$t_{int} = 60s$	$t_{int} = 120s$
$p_{x1s}, p_{y1s}, p_{z1s}$	20.56	15.12	6.32
$p_{x2s}, p_{y2s}, p_{z2s}$	52.01	28.53	23.26
$a_{x1s}, a_{y1s}, a_{z1s}$	0.37	0.18	0.08
$a_{x2s}, a_{y2s}, a_{z2s}$	0.67	1.05	1.27

Optimum filter parameter values for a sample matrix  $M_s$  250, 250, 250 with a meshgrid resolution of 2 mm  $\times$  2 mm  $\times$  2 mm.

TABLE II

Material Properties of the Body Tissues

Tissue	$W(\text{ml/min/kg})$	$\rho(\text{kg/m}^3)$	$c_p(\text{J/kg/C}^\circ)$	$k(\text{W/m/C}^\circ)$	$Q(\text{W/kg})$
Blood	10000	1050	3617	0.52	0
Cancellous bone	30	1178	2274	0.31	0.46
Cartilage	35	1100	3568	0.49	0.54
Cerebellum	770	1045	3653	0.51	15.67
Cortical bone	10	1908	1313	0.32	0.15
CSF	0	1007	4096	0.57	0
Fat	33	911	2348	0.21	0.51
Grey Matter	763	1045	3696	0.55	15.53
Muscle	39	1090	3421	0.49	0.96
Nerve	160	1075	3613	0.49	2.48
Sclera	380	1032	4200	0.58	5.89
Skin	106	1109	3391	0.37	1.65
Tendon	29	1142	3432	0.47	0.45
Tongue	78	1090	3421	0.49	1.21
Vitreous humor	0	1005	4047	0.59	0
White Matter	213	1041	3583	0.48	4.34

Material properties of the body tissues.